Accelerated evolution of convective simulations

Evan H. Anders and Benjamin P. Brown
Dept. Astrophysical & Planetary Sciences, University of Colorado – Boulder, Boulder, CO 80309, USA and Laboratory for Atmospheric and Space Physics, Boulder, CO 80303, USA

Jeffrey S. Oishi
Department of Physics and Astronomy, Bates College, Lewiston, ME 04240, USA

We present a method for coupling boundary value problems with initial value problems in order to achieve Accelerated Evolution (AE) of convective solutions on dynamical timescales, rather than the long thermal timescale. We study this method in the context of Rayleigh-Bénard convection. We demonstrate that the solution reached by AE and Standard Evolution (SE) are similar, and that this method works at a large range of supercriticalities. The AE method is used to achieve converged solutions at high supercriticality (10^7), and its extensions to more complex systems are briefly discussed.

I. INTRODUCTION

Natural convection occurs in the presence of disparate timescales which prohibit numericists from studying realistic models of natural systems. For example, flows in the convection zones of stars like the Sun are characteristically low Mach number (Ma) in the deep interior. Explicit timestepping methods which are bound by the Courant-Friedrich-Lewy (CFL) timestep limit must resolve the fastest motions (sound waves), resulting in timesteps which are prohibitively small for studies of the deep, low-Ma motions. These systems are numerically stiff, and the difference between the sound crossing time and the convective overturn time have made studies of low-Ma stellar convection difficult. Traditionally, approximations such as the anelastic approximation, in which sound waves are explicitly filtered out, have been used to study low-Ma flows [1, 2]. More recently, advanced numerical techniques which use implicit or mixed implicit-explicit timestepping mechanisms have made it feasible to study convection at low Mach numbers [3–8], and careful studies of deep convection which would have been impossible a decade ago are now widely accessible.

Convective systems with divergent dynamical timescales can now be studied; however, thermal timescales, which characterize system relaxation, are often much larger than dynamical timescales, and resolving dynamics in atmospheres which are sufficiently thermally relaxed remains a challenging problem. Solar convection is a prime example of this phenomenon. Dynamical timescales in the solar convective zone are relatively short (10 min overturn at solar surface, one month solar rotation rate) compared to the Sun's Kelvin-Helmholtz timescale of $3 \cdot 10^7$ years [9]. In such a system, it is impossible to resolve the convective dynamics while also evolving the thermal structure of the system in a meaningful fashion using traditional timestepping techniques alone. As modern simulations aim to model natural convection by increasing into the high-Rayleigh-number (Ra) regime, the thermal diffusion timescale becomes intractably large compared to dynamical timescales [7]. Furthermore, as dynamical and thermal timescales separate, simulations become more turbulent. Increasingly turbulent motions require finer grid meshes and smaller timesteps to capture advective dynamics. Thus, the progression of simulations into the high-Ra regime of natural convection is slowed by two simultaneous effects: timestepping through a single convective overturn time becomes more computationally expensive and the number of overturn times required for systems to reach thermal equilibration grows.

The vast difference between convective and thermal timescales has long plagued numericists studying convection, and an abundance of approaches has been employed to study thermally converged solutions. One popular method for accelerating the convergence of high-Ra solutions is by "bootstrapping" – the process of using the flow fields in a converged solution at low Ra as initial conditions for a simulation at high Ra. This method has been used with great success [10, 11], but it is not without its faults. Bootstrapped solutions are succeptible to hysteresis effects, in which large-scale convective structures present in the low Ra solution imprint onto the dynamics of the new, high Ra solution. Another commonly-used tactic in moderate-Ra simulations is to use a simple model of the full convective state as initial conditions. For example, past studies have used a linear eigenvalue solve to set the initial convective state [12] or used an axisymmetric solution as initial conditions for convection in a 3D cylinder [11]. In other systems, the approximate state of the evolved solution can be estimated. There, a set of initial conditions which is close to the evolved state be derived analytically [13, 14].

Despite the numerous methods that have been used, the most straightforward way to achieve a thermally converged solution is to evolve a convective simulation through a thermal timescale. Some modern studies do just that [2]. However, such evolution is *expensive*, and state-of-the-art simulations at the highest values of Ra can only reasonably

be run for tens to hundreds of buoyancy times [15], much less the thousands of buoyancy timescales required for thermal convergence.

In this work, we study a method of achieving accelerated evolution of convective simulations. We couple measurements of the dynamics of non-converged convective simulations with knowledge about energy balances in the desired solution to self-consistently adjust the mean thermodynamic profile towards its evolved state. While such a method has been used previously [16], we find no explanation in the current literature of the steps involved in employing this method, nor any study into the accuracy of such a method. In section II, we describe our convective simulations, our numerical methods, and our method for achieving accelerated evolution. In section III, we compare solutions reached through the accelerated evolution method to those that have been evolved through a full diffusive timescale, and we examine select simulations at high Ra which have achieved accelerated evolution. Finally, in section IV, we discuss extensions of the methods presented here, and we offer concluding remarks.

II. EXPERIMENT

We study incompressible Rayleigh-Bénard convection under the Oberbeck-Boussinesq approximation, such that our fluid has a constant kinematic viscosity (ν), thermal diffusivity (κ), and coefficient of thermal expansion (α). The density of the fluid is a constant, ρ_0, except where it is $\rho = \rho_0(1-\alpha T_1)$ on the term where the constant gravitational acceleration, $\boldsymbol{g} = -g\hat{z}$, acts in the vertical momentum equation. The equations of motion are [17]

$$\nabla \cdot \boldsymbol{u} = 0, \tag{1}$$

$$\frac{\partial \boldsymbol{u}}{\partial t} + \boldsymbol{u}\cdot\nabla\boldsymbol{u} = -\frac{1}{\rho_0}\nabla P - g(1-\alpha T_1)\hat{z} + \nu\nabla^2\boldsymbol{u}, \tag{2}$$

$$\frac{\partial T_1}{\partial t} + \boldsymbol{u}\cdot\nabla(T_0+T_1) = \kappa\nabla^2 T_1, \tag{3}$$

where $\boldsymbol{u} = u\hat{x} + v\hat{y} + w\hat{z}$ is the velocity, $T = T_0 + T_1$ are the initial and fluctuating components of temperature, and P is the pressure. We non-dimensionalize these equations such that the length is in units of the layer height (L_z), temperature is in units of the initial temperature jump across the layer ($\Delta T_0 = L_z\nabla T_0$), and velocity is in units of the freefall velocity ($v_{\rm ff} = \sqrt{\alpha g L_z^2 \nabla T_0}$). by these choices, one time unit is a freefall time ($L_z/v_{\rm ff}$). We introduce a reduced kinematic pressure, $\varpi \equiv (P/\rho_0 + \phi + |\boldsymbol{u}|^2/2)/v_{\rm ff}^2$, where the gravitational potential, ϕ, is defined such that $\boldsymbol{g} = -\nabla\phi$. As P is a Langrange multiplier under the Oberbeck-Boussinesq approximation, ϖ can be treated straightforwardly as a linear variable. In non-dimensional form, Eqns. 2 & 3 become

$$\frac{\partial \boldsymbol{u}}{\partial t} + \nabla\varpi - T_1\hat{z} + \mathcal{R}\nabla\times\boldsymbol{\omega} = \boldsymbol{u}\times\boldsymbol{\omega}, \tag{4}$$

$$\frac{\partial T_1}{\partial t} - \mathcal{P}\nabla^2 T_1 + w\frac{\partial T_0}{\partial z} = -\boldsymbol{u}\cdot\nabla T_1, \tag{5}$$

where $\boldsymbol{\omega} = \nabla\times\boldsymbol{u}$ is the vorticity. The dimensionless control parameters $\mathcal{P}$ and $\mathcal{R}$ are set by the Rayleigh and Prandtl numbers,

$$\mathcal{R} \equiv \sqrt{\frac{\rm Pr}{\rm Ra}}, \qquad \mathcal{P} \equiv \frac{1}{\sqrt{\rm Pr\,Ra}}, \qquad {\rm Ra} = \frac{g\alpha L_z^4 \nabla T_0}{\nu\kappa} = \frac{(L_z\, v_{\rm ff})^2}{\nu\kappa}, \qquad {\rm Pr} = \frac{\nu}{\kappa}. \tag{6}$$

We hold Pr= 1 constant throughout this work, such that $\mathcal{P} = \mathcal{R}$.

We study 2D and 3D convection in which the domain is a cartesian box, whose dimensionless vertical extent is $z \in [-1/2, 1/2]$, and which is horizontally periodic with an extent of $x, y \in [0, \Gamma]$, where $\Gamma = 2$ is the aspect ratio. In 2D simulations, we set $v = \partial_y = 0$. We specify no-slip, impenetrable boundary conditions at both the top and bottom boundary and we use mixed thermal boundary conditions, such that

$$u = v = w = 0 \text{ at } z = \pm 1/2, \qquad T_1 = 0 \text{ at } z = +1/2, \qquad \frac{\partial T_1}{\partial z} = 0 \text{ at } z = -1/2. \tag{7}$$

For this choice of boundary conditions, the critical value of Ra at which the onset of convection occurs is ${\rm Ra_{crit}} = 1295.78$, and the supercriticality of a run is defined as $S \equiv {\rm Ra/Ra_{crit}}$. Studies of convection which aim to model astrophysical systems such as stars often employ mixed thermal boundary conditions [12, 18, 19], as we do here; however, our choice of thermal boundary conditions here reflects the fact that the conditions in Eqn. (7) are the simplest to implement in the process of accelerated evolution (see section II A) we study here.

We utilize the Dedalus[1] pseudospectral framework [20] to evolve Eqns. (1), (4), & (5) forward in time using an implicit-explicit (IMEX), third-order, four-step Runge-Kutta timestepping scheme RK443 [21]. The linear terms (on the LHS of the equations) are solved implicitly, while the nonlinear terms (RHS) are explicitly solved. Variables are time-evolved on a dealiased Chebyshev (vertical) and Fourier (horizontal, periodic) domain in which the physical grid dimensions are 3/2 the size of the coefficient grid.

As initial conditions, we fill T_1 with random white noise whose magnitude is $10^{-6}\mathcal{P}$. This ensures that the initial perturbations are much smaller than the evolved convective temperature perturbations, even at large Ra. We filter this noise spectrum in coefficient space, such that only the lower 25% of the coefficients have power.

A. The method of Accelerated Evolution

Here we describe a method of Accelerated Evolution (AE), which we use to rapidly evolve the thermodynamic state of convective simulations. We compare this AE method to Standard Evolution (SE), in which we naively evolve the atmosphere for one thermal diffusion time, $t_\kappa = \mathcal{P}^{-1}$. As Ra increases, SE solutions become intractable, while the timeframe of convergence for an AE solution remains nearly constant in freefall time units. For an example of time saving achieved by using AE, we compare energy traces at $S = 10^5$ from a SE run in Fig. 1a to an AE run in Fig. 1c.

The horizontally averaged profiles of the vertical conductive flux, $\mathrm{F}_{\mathrm{cond}} = \langle -\kappa\nabla(T_0 + T_1)\rangle_{x,y}$, and the vertical convective flux, $\mathrm{F}_{\mathrm{conv}} = \langle w(T_0 + T_1)\rangle_{x,y}$, where $\langle\rangle_{x,y}$ represent a horizontal average, are the basis of the AE method. We measure both of these quantities early in a simulation, retrieving profiles similar to those shown in Fig. 1b. At early stages in the simulation, these flux profiles are highly asymmetric, with more flux exiting the atmosphere at the upper boundary than the fixed-flux lower boundary is providing. By calculating the total flux, $\mathrm{F}_{\mathrm{tot}} = \mathrm{F}_{\mathrm{conv}} + \mathrm{F}_{\mathrm{cond}}$, we derive the profiles

$$f_{\mathrm{conv}}(z) = \frac{F_{\mathrm{conv}}}{F_{\mathrm{tot}}}, \qquad f_{\mathrm{cond}}(z) = \frac{F_{\mathrm{cond}}}{F_{\mathrm{tot}}}, \tag{8}$$

which have the systematic asymmetries removed. These profiles describe which parts of the atmosphere depend on convection to carry flux (where $f_{\mathrm{conv}}(z) = 1$ and $f_{\mathrm{cond}}(z) = 0$). We presume that the early convection occupies roughly the same volume as the evolved convection, and thus that the extent of the early thermal boundary layers (where $f_{\mathrm{cond}}(z) = 1$ and $f_{\mathrm{conv}}(z) = 0$) will not change significantly over the course of the atmosphere's evolution. Under this assumption, the proper evolved atmospheric flux profiles are $\mathrm{F}_{\mathrm{conv,\,ev}} = \mathrm{F}_{\mathrm{bot}} \cdot f_{\mathrm{conv}}$ and $\mathrm{F}_{\mathrm{cond,\,ev}} = \mathrm{F}_{\mathrm{bot}} \cdot f_{\mathrm{cond}}$, where $\mathrm{F}_{\mathrm{bot}} = \mathcal{P}$ is the amount of flux entering the bottom of the atmosphere.

In a time-stationary state, the horizontal- and time-average of Eqns. (4) and (5), neglecting terms which vanish due to symmetry, are

$$\frac{\partial}{\partial z}\langle\varpi\rangle_{x,y} - \langle T_1\rangle_{x,y}\,\hat{z} = \langle \boldsymbol{u}\times\boldsymbol{\omega}\rangle_{x,y}\,, \tag{9}$$

$$\frac{\partial}{\partial z}\mathrm{F}_{\mathrm{conv,\,ev}} - \mathcal{P}\frac{\partial^2}{\partial z^2}\langle T_1\rangle_{x,y} = 0. \tag{10}$$

Convective flows are perturbations around a thermal profile defined by these equations in the proper evolved, statistically stationary state. Furthermore, under the specification of $\mathrm{F}_{\mathrm{conv,\,ev}}$ and $\langle \boldsymbol{u}\times\boldsymbol{\omega}\rangle_{x,y}$, *the mean thermodynamic structure of the system is fully specified.*

Thus, the AE method is simple: we construct $\mathrm{F}_{\mathrm{conv,\,ev}}$ as described above. Then we calculate a profile, $\xi(z) = \mathrm{F}_{\mathrm{conv,\,ev}}/\mathrm{F}_{\mathrm{conv}}$, which is the fraction, as a function of height, by which the flux in the system must be reduced to go from an initial state (Fig. 1b) to an evolved state (Fig. 1d). We multiply the velocities and the thermal fluctuations, $T - \langle T\rangle_{x,y}$, by $\sqrt{\xi}$, such that the advected, flux-carrying perturbations in the temperature are appropriately diminished. We then solve a boundary value problem including Eqns. (9) & (10) using $\mathrm{F}_{\mathrm{conv,\,ev}}$ and $\cdot\,\langle \boldsymbol{u}\times\boldsymbol{\omega}\rangle_{x,y}$, after diminishing it by a factor of ξ. We use mixed thermal boundary conditions, as in Eqn. (7), because F_{bot} is exactly specified, and the temperature profile is pegged at a reference value for the AE solve. For specifics on the precise implementation of the AE method, we refer the reader to appendix A.

The AE method converges atmospheres from extreme flux disequilibrium states (Fig. 1b) on short dynamical timescales (Fig. 1c) to a converged state (Fig. 1d) whose flux balance is very close to the balance present in the corresponding SE solution (Fig. 1e). While the application of the AE method advances solutions toward the proper solution, we find that multiple applications of the method is the best means of achieving converged solutions quickly.

---

[1] http://dedalus-project.org/

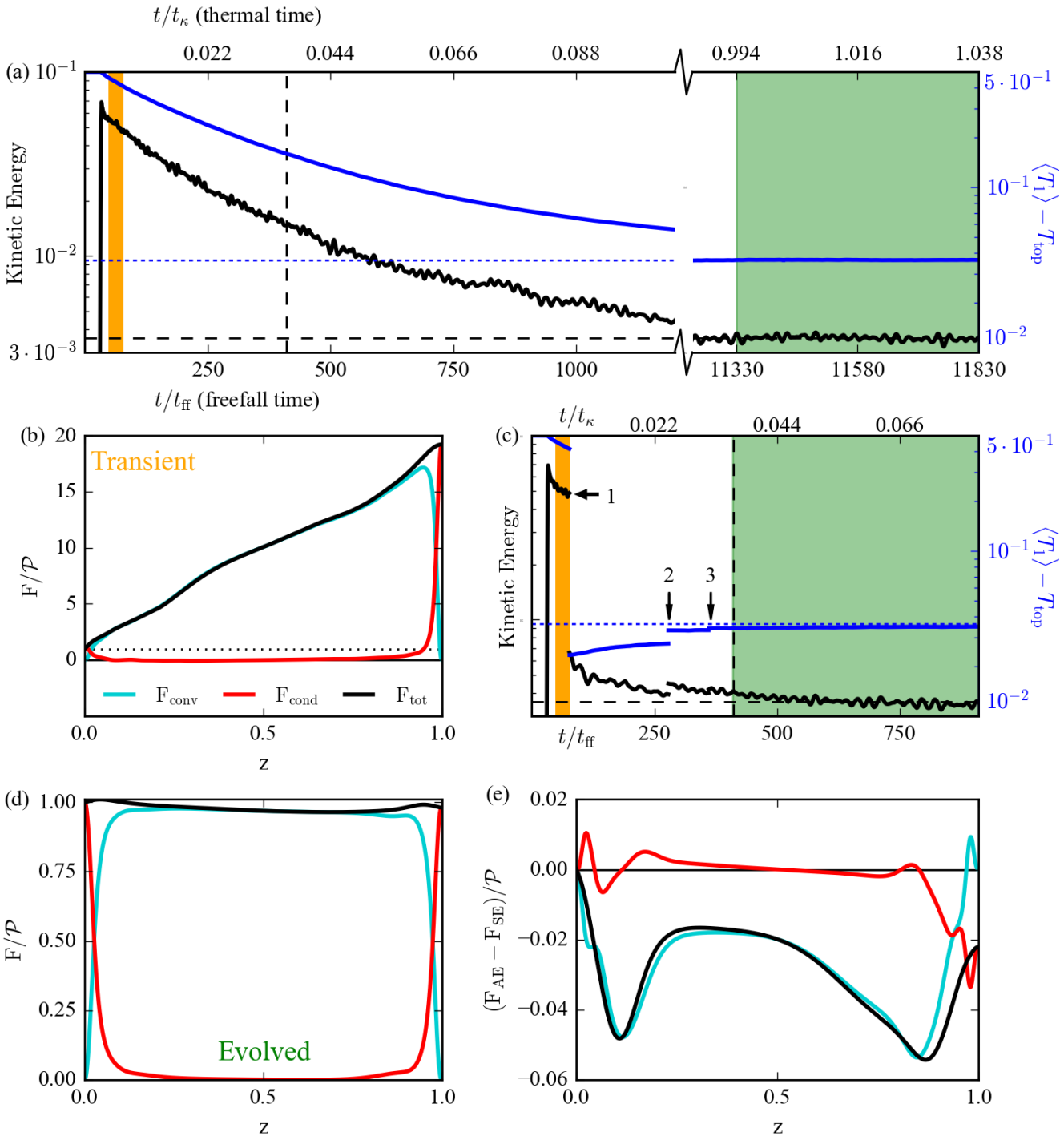

FIG. 1. (a) Kinetic energy (black) and mean temperature (blue) vs. time are shown for a SE run at $S = 10^5$. The mean evolved values of kinetic energy and mean temperature, averaged over the time shaded in green, are denoted by the horizontal dashed lines. (b) The time- and horizontally-averaged flux profiles are shown for the times highlighted in orange in (a). (c) The same quantities as in (a) are shown, but for AE at the same parameters. The axes are scaled identically in (a) and (c), and the AE method is used three times, marked by the numbered arrows in (c). The fluxes averaged over the green shaded region of (c) are shown in (d). The difference between the fluxes in the AE and SE solutions is shown in (e). The dashed vertical line in (a) and (c) denotes the simulation time at which evolved measurements are started for the AE case.

III. RESULTS

We study evolved solutions achieved through the standard evolution (SE) method from convective onset up to $S = 10^5$ in 2D and $S = 10^4$ in 3D. These SE runs are compared to accelerated evolution (AE) runs spanning from onset up to $S = 10^7$ in 2D and $S = 10^4$ in 3D. For a full list of simulations, we refer the reader to appendix B.

We report the time- and volume-averaged values of select measurements of the evolved solutions in Fig. 2. The scaling of heat transport in the evolved solution, as quantified by the Nusselt number, is shown in Fig. 2a. The volume averaged Nusselt number is defined as

$$\mathrm{Nu} = \frac{\langle F_{\mathrm{conv}} + F_{\mathrm{cond}} \rangle}{\langle F_{\mathrm{cond,\ ref}} \rangle} = \frac{\langle wT - \mathcal{P}\partial_z T \rangle}{\langle -\mathcal{P}\partial_z T \rangle}, \tag{11}$$

where $\langle\rangle$ represent a volume average. In 2D when $S < 10^{3+2/3}$ and in 3D, the evolved system is defined by a clear value of Nu and the convective heat transport reaches a temporally stationary state. In 2D and at larger values of S, the value of Nu oscillates as a function of time due to large horizontal oscillations in the convective plume structures. Our choice of no-slip boundary conditions prevent the fluid from entering a shearing state [22], but the oscillatory motions which do arise cause the system to vary between periods of low heat transport and high heat transport. The SE simulations which span up to $S = 10^5$ exhibit the same horizontally oscillatory motion as the AE solutions for the same initial conditions. The scaling of the mean value of Nu is roughly $\mathrm{Nu} \propto \mathrm{Ra}^{1/5}$, weaker than that reported in similar systems with fixed-T and fixed-flux boundary conditions [10]. We attribute this weaker Nu scaling to the oscillatory nature of the plumes, which may have been avoided by previous studies using bootstrapping techniques as initial conditions.

In Fig. 2b, we report the volume-averaged RMS Reynolds number in the AE solutions, where $\mathrm{Re} = \langle |\boldsymbol{u}| \rangle / \mathcal{R}$. This measure scales roughly as $\mathrm{Re} \propto \mathrm{Ra}^{0.45}$, and shows little variance with time.

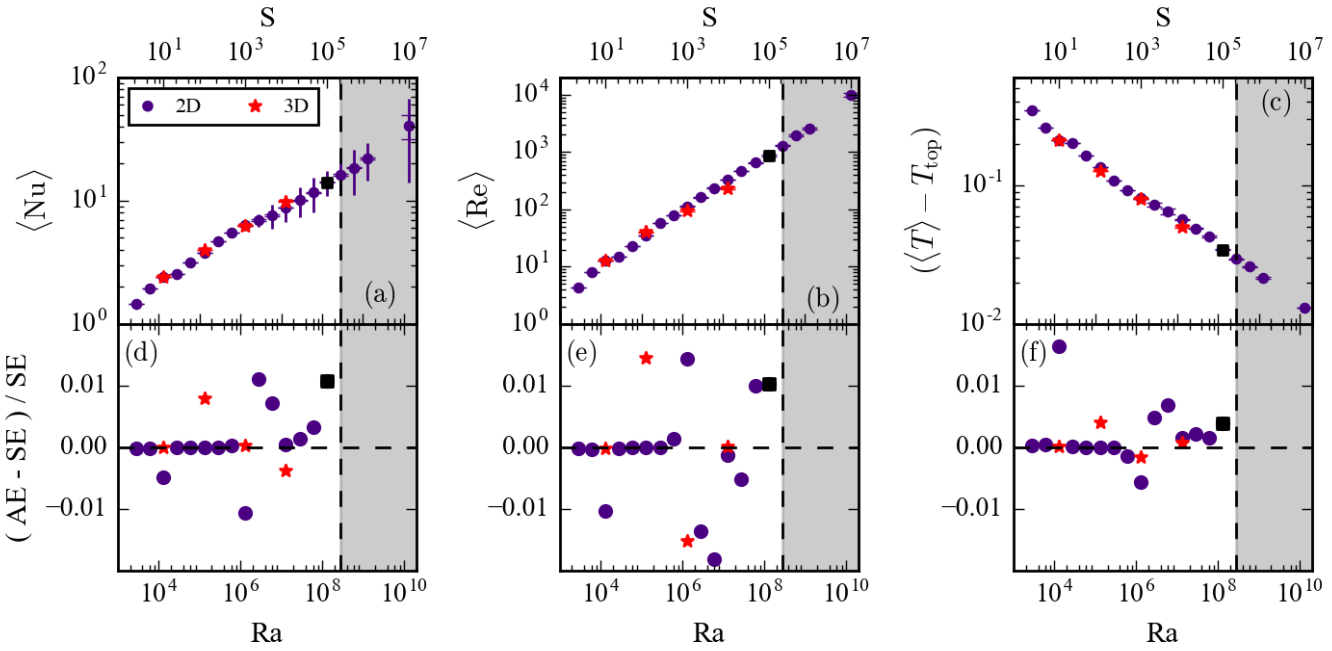

FIG. 2. Volume- and time-averaged measurements of the Nusselt number (Nu), the RMS Reynolds number (Re), and the mean temperature ($\langle T \rangle$) for AE runs are shown in (a)-(c). Symbols are located at the mean value of each measurement. Vertical lines represent the standard deviation of the measurement, and quantify natural variation over the averaging window. Error bars represent the change in the mean value over the averaging window, such that very large error bars represent solutions which are not fully converged when averaging begins. (a) Nu scales as $\mathrm{Ra}^{1/5}$; above $\mathrm{S} \geq 10^{3+2/3}$, simulations exhibit oscillating plume structures whose heat transport fluctuates over time. (b) Re, which measures the level of turbulence in the evolved solution, scales as $\mathrm{Ra}^{0.45}$. (c) The difference between $\langle T \rangle$ and the value of T at $z = +1/2$ is shown, and this quantity scales as $\mathrm{Ra}^{-1/5}$, the inverse of Nu. Relative error for measurements of (d) Nu, (e) Re, and (f) T between AE solutions and SE solutions are shown. The greyed area of the plots indicates the region in which only AE runs were carried out due to computational expense. The run at $S = 10^5$ marked as a black square is examined in more details in Figs. 1, 3, & 4.

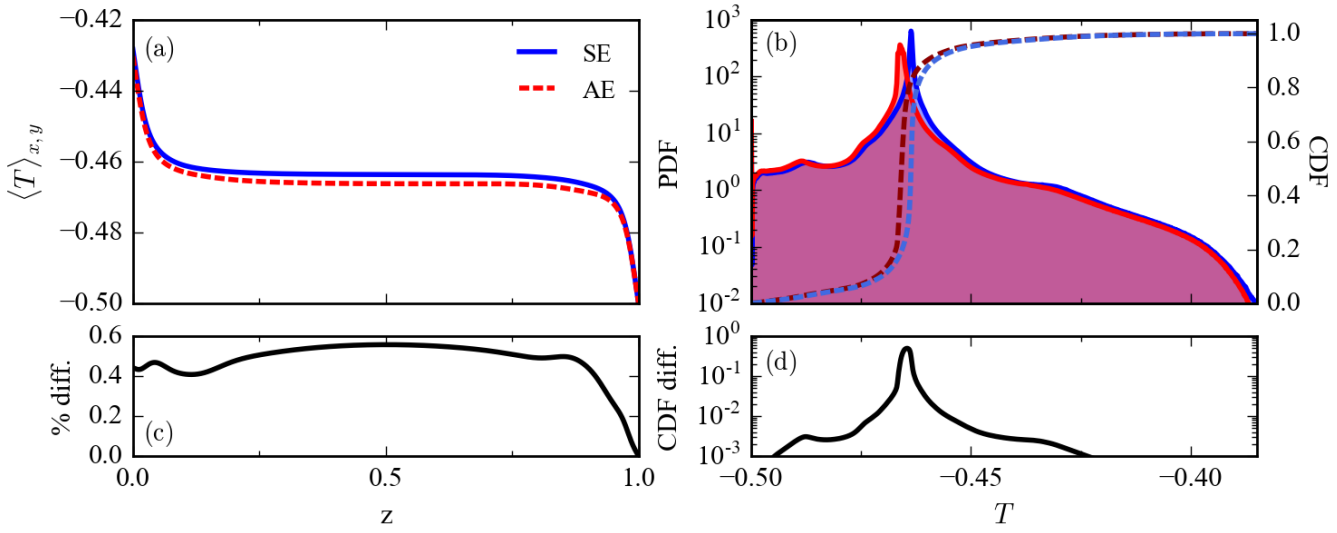

FIG. 3. Comparisons of the evolved thermodynamic states of an AE and SE run at $S = 10^5$ are shown. (a) Evolved horizontally- and time-averaged temperature profiles, as a function of height. (b) Probability Distribution Functions (PDFs) and their integrated Cumulative Distribution Functions (CDFs) of point-by-point measurements of the temperature field. T is sampled every 0.1 time units for 500 total time units, and was interpolated onto an evenly spaced grid before sampling. (c) The percentage difference between the mean temperature profiles as a function of height. The difference between the mean profiles is very small, O(0.5%). (d) The value of the Kolmogorov-Smirnov (KS) statistic, or the difference between the AE and SE CDFs, as a function of temperature. The small difference in the interior temperature results in a large difference between the two temperature CDFs near the values of the temperature modes. The spread of temperature around the modes, which includes the fluctuations that drive convection, are nearly identical between the two runs.

In Fig. 2c, we report the volume averaged temperature of the AE solutions, with the value at the upper (fixed T) boundary removed. This measurement probes the thickness of the boundary layers of the solutions, and should show scaling which is inversely proportional to Nu in converged solutions where fixed-flux boundary conditions are used [23]. We find here that $(\langle T \rangle - T_{\text{top}}) \propto \text{Ra}^{-1/5}$, precisely the inverse scaling of Nu, giving confidence that these solutions are in a converged state.

In Fig. 2d-f, we report the fractional difference between measurements from the AE solutions and measurements from the SE solutions. We find that the mean value of Nu from AE solutions is accurate to the values from SE solutions to within $\sim 1\%$, and the same is true for $\langle T \rangle$ measurements. Re measurements show slightly greater error, with AE measurements being on average $\leq 2\%$ away from the SE measurements.

The measurements presented in Fig. 2 demonstrate that the AE method can be powerfully employed in parameter space studies in which large numbers of simulations are compared in a volume-averaged sense. We now turn our examination to a more direct comparison of AE and SE for convection at $S = 10^5$, as has been introduced in Fig. 1.

As the AE method primarily serves to adjust the thermodynamic structure of the solution, we compare the temperature profile attained by AE and SE in Fig. 3. We see that the boundary layer length scale is nearly identical between the two solutions (Fig. 3a), but that the mean temperature in the interior differs by about 0.5% on average (Fig. 3c).

The probability distribution functions of point-by-point temperature measurements are compared for the two runs in Fig. 3b. We construct this PDF from snapshots of the temperature profile every 0.1 freefall time units over a duration of 500 total freefall time units, as shown by the green areas if Fig. 1a&c. We interpolate the temperature field of each of these snapshots onto an evenly spaced grid, determine the frequency distribution of all measured T values, and then normalize the distribution such that its integral is unity. The primary difference between the two PDFs is their modes, which is expected from Fig. 3a. The fact that the the AE temperature profile is roughly 0.5% off of the SE temperature profile (3c), the AE temperature field is still marginally evolving towards the SE temperature field, and this evolution appears as asymmetry of the AE PDF's peak.

One means of comparing two probability distributions to determine if they are drawn from the same underlying sample is through the use of a Kolmogorov-Smirnov (KS) [24]. In general, a KS test must be conducted on independent, uncorrelated data, which poorly describes the point-by-point values of flow in a fluid simulation. Thus, we will merely use the KS statistic, the maximum difference between the cumulative distribution functions (CDFs) of the two sample distributions, as a numerical method of directly comparing the two PDFs. For the distributions shown in Fig. 3b,

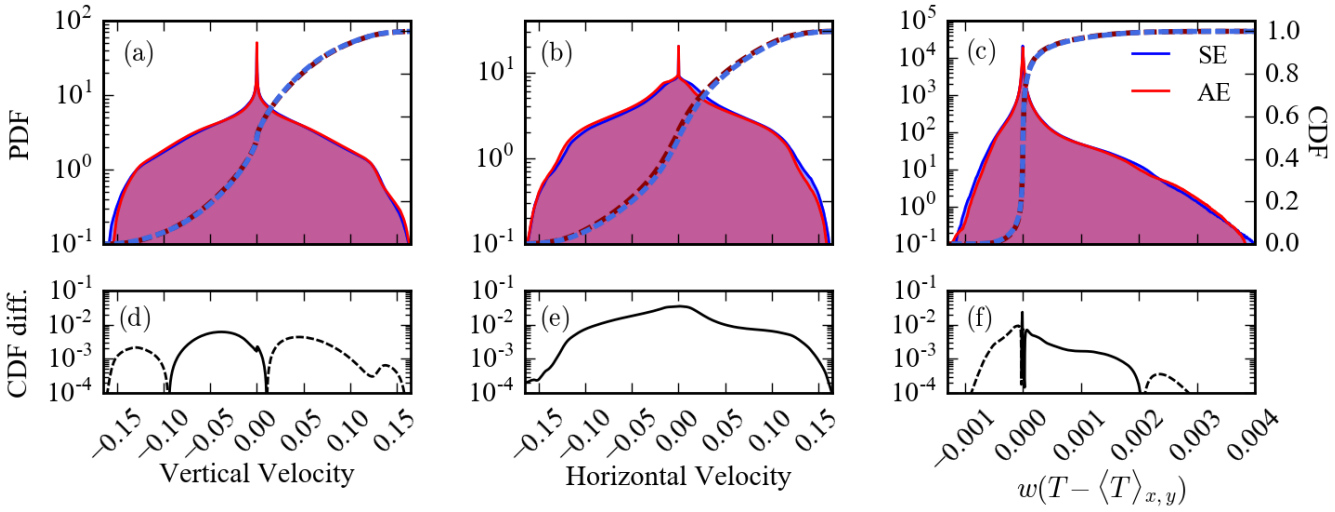

FIG. 4. Probability distribution functions (PDFs) of (a) the vertical velocity, (b) the horizontal velocity, and (c) nonlinear convective transport are shown for 2D runs achieved through SE (blue) and AE (red) at $S = 10^5$. Flows are sampled every 0.1 time units for 500 total time units, and are first interpolated onto an evenly spaced grid. The cumulative distribution function (CDF) is overplotted for each PDF. (d-f) The KS statistics, or the values of $\mathrm{CDF_{AE}}$ - $\mathrm{CDF_{SE}}$, are shown for the related distributions, and solid lines indicated positive values while dashed lines are negative values. Unlike the temperature distributions in Fig. 3, these distributions, particularly the vertical velocity and transport, show very good agreement and small values of the KS statistic.

the difference between the CDFs is shown in Fig. 3d. The maximum difiference, or the KS statistic, is 0.495 near the modes. This difference is very large, but is not unexpected. While the temperature distributions near the modes are very different, their spread of perturbations is nearly identical.

In addition to comparing the thermodynamic state achieved by the SE and AE methods, we examine the velocities found in the evolved states. We compute PDFs in the same manner as in Fig. 3b for the vertical velocity (Fig. 4a), horizontal velocity (Fig. 4b), and the nonlinear convective flux (Fig. 4c). We report KS statistics of 0.00615, 0.0349, and 0.0263, respectively. Perhaps unsurpisingly, the nonlinear convective transport between the SE and AE methods are very similar, as is captured in a volume-averaged sense in the Nu measurements of Fig. 2a&d. Each distribution shows a strong peak near zero due to the velocity boundary conditions (Eqn. (7)), but the distribution of flux transport elements and velocities is nearly identical in the AE and SE solutions.

The small differences between the SE and AE solutions for the case studied in Figs. 1, 3, & 4, show that the AE method is extremely powerful. The first application of the AE method ($t \approx 70$ in Fig. 1b) immediately increases the average time step of our solver by a factor of 2-3. At higher supercriticality ($S = 10^7$), the AE solve immediately boosts the timestep by nearly a factor of 4. Thus, not only does this method evolve the solution into nearly the correct state, but further time evolution (either to achieve precisely the correct thermodynamic state or to take measurements of fluid quantities) happens more efficiently.

IV. EXTENSIONS & CONCLUSION

In this work, we have studied a method of Accelerated Evolution (AE) which can be employed to achieve rapid thermal convergence of convective simulations. We compared this technique to the Standard Evolution (SE) of convection through a thermal diffusion timescale and showed that AE rapidly obtains solutions whose dynamics are similar to SE solutions. The AE method is not only valid at low values of S, where SE solutions converge quickly due to the short thermal timescale, but AE is also applicable at high values of S, where SE solutions are intractable. We have studied the AE method in both 2D and 3D, but restricted most of our study to 2D flows; AE depends only on the 1D horizontal average of quantities, and our inclusion of 3D simulations was merely to demonstrate the broadly useful nature of AE.

Here we studied Rayleigh-Bénard convection as a test case for the AE method, but we argue that the true power of this technique is in its extensions to more complicated studies. To achieve AE in more complicated systems, one need only derive the steady-state, horizontally-averaged equations governing the convective dynamics (e.g., Eqns. (9)

& (10)) and couple those equations with knowledge of the boundary conditions and current dynamics as described in section II A and appendix A. While in-depth studies of AE extensions are beyond the scope of this paper, we will briefly discuss avenues in which the AE method should be explored and tested.

Convection in natural systems is often driven by internal heating processes rather than imposed, fixed boundary condditions. The AE procedure can be straightforwardly applied to Boussinesq studies of internally heated convection [25], where a constant source term in the energy equation causes the vertical flux through the system to increase with height. These systems can be straightforwardly studied using exactly the methods that we examined here, but scaling the flux profiles derived in Eqn. (8) by the proper, height-dependent flux. Studies of convection in natural system often employ height-dependent conductivities [26], leading to natural flux divergences that act as internal heating terms, and the study of this method in the simple internal heating context will be an important step towards achieving AE in simulations with astrophysically realistic conductivities.

In order to understand the influences of overshooting convection, some studies examine adjacent stable and convecting regions [13, 14, 16]. When the interface between the stable region and the convecting region is stiff and motions do not cross that interface, convective motions cannot accelerate the restratification of the stable region. In fully-convective domains, such as those studied in this work, the thermodynamics evolve at a more rapid rate than the thermal diffusion time across the domain due to the help of convective motions. For example, in Fig. 1a, the SE solution is fully converged after $4 \cdot 10^3$ frefall time units, despite the thermal timescale being roughly 10^4 freefall units. However, in studies where there is a stable region which is not mixed by convection, the experimentalist must either wait through a thermal diffusion time for the region to restratify or employ methods such as the AE method to study evolved atmospheres.

Studies of stratified, compressible convection have much to gain through developing and employing AE. In many studies of stratified convection, the thermal diffusivity is inversely proportional to the density [7]. Thus, the thermal timescale grows with depth in the atmosphere, and the difficulty of achieving thermal convergence grows as simulators study more highly stratified domains. In order to extend AE into this regime, two additional pieces of information must be considered. First, rather than constructing the profiles in Eqn. (8) with the total flux through the domain, only the superadiabatic portion of the flux should be considered. Second, in addition to solving for hydrostatic balance and thermal equilibrium, as in Eqns. (9) & (10), it is essential to simultaneously evolve the density profile in a manner which conserves mass. In a 1D boundary value problem, such as is solved to achieve AE here, this implies the inclusion of an equation which tracks the vertically integrated mass, and sets boundary conditions on that mass to ensure that no mass enters or leaves the domain.

An eventual use case of AE is in robustly replacing Mixing Length Theory (MLT) in stellar evolution codes. Current state of the art stellar structure models are the solutions of 1D simulations which parameterize convection using MLT [27]. Recent work has taken the first steps towards understanding how to simultaneously resolve convective motions while evolving systems through many thermal timescales, as is required in the evolution of stars. We now know that implicit timestepping methods, while not technically bound by CFL constraints, must resolve the convective motions for stability [3–5], and are thus not an ideal solution to achiving long-term system evolution. Recently, efforts have begun to improve 1D models of stellar convection by projecting the results of 3D simulations into 1D to more properly parameterize convection [28, 29]. This is precisely an extension of the AE that we present here, and through the careful addition and testing of new physics, AE shows great potential for improving our understanding of convection in general, and stellar evolution models in particular.

ACKNOWLEDGMENTS

EHA acknowledges the support of the University of Colorado's George Ellery Hale Graduate Student Fellowship. This work was additionally supported by NASA LWS grant number NNX16AC92G. Computations were conducted with support by the NASA High End Computing (HEC) Program through the NASA Advanced Supercomputing (NAS) Division at Ames Research Center on Pleiades with allocations GID s1647 and GID g26133.

Appendix A: Accelerated Evolution Recipe

In order to achieve Accelerated Evolution (AE), we pause the Direct Numerical Simulation (DNS) which is evolving the dynamics of the convection and solve a 1D Boundary Value Problem (BVP) consisting of Eqns. (9) & (10). After solving this BVP, we adjust the fields being evolved in the DNS appropriately towards their evolved state, and then we continue running the now-evolved DNS. There specific steps taken in completing the AE method are as follows:

1. After the start of the DNS, we wait some time, $t_{\text{transient}}$ after the convective transient in which the dynamics vigorously break away from the hydrostatic state.

2. Then, during the DNS, we calculate time averages of the 1D profiles of $F_{\rm conv}$, $F_{\rm tot}$, and $\langle \boldsymbol{u} \times \boldsymbol{\omega} \rangle_{x,y}$, updating them every timestep. To calculate these averages, we use a trapezoidal-rule integration in time, and then divide by the total time elapsed over which the average is taken.

3. We pause the DNS once the averages are sufficiently converged. To ensure that an average is converged, at least some time $t_{\rm min}$ must have passed since the average was started to ensure that the full range of convective dynamics are probed, and the profiles must change by no more than P% on a given timestep.

4. Construct $\mathrm{F}_{\rm conv,\ ev}$ and ξ as specified in section II A from the averaged profiles.

5. Solve the BVP for $\langle T_1 \rangle_{x,y}$ and $\langle \varpi \rangle_{x,y}$ of the evolved state. Set the horizontal average of the current DNS thermodynamic fields equal to the results of the BVP.

6. Multiply the velocity field and the temperature fluctuations, $T - \langle T \rangle_{x,y}$, by $\sqrt{\xi}$ in the DNS to properly reduce the convective flux.

7. Continue running the DNS

We refer to this process as an "AE BVP solve."

While the use of a single AE BVP solve rapidly advances the convecting state to one that is closer to the evolved state, we find that repeating this method multiple times is the best way to ensure that the AE solution is truly converged. For all runs in 2D at $S < 10^5$, we set $t_{\rm transient} = 50$, completed an AE BVP solve with $t_{\rm min} = 30$ and $P = 0.1$, and then repeated the procedure, including another wait of $t_{\rm transient} = 50$ before beginning averages. For all 3D runs and 2D runs with $S \in [10^5, 10^6]$, we did a first AE BVP solve with $t_{\rm transient} = 20$, $t_{\rm min} = 20$, and $P = 1$ in order to quickly reach a near- converged state and vastly increase our timestep size. After this first solve, we completed two AE BVP solves, with $t_{\rm transient} = 30$, $t_{\rm min} = 30$, and $P = 0.1$ to get very close to the solution (as in Fig. 1c). At very high $S = 10^7$, we ran two AE BVP solves with $t_{\rm min} = 20$ and $P = 1$. For the first solve, we set $t_{\rm transient} = 20$, and for the second we set $t_{\rm transient} = 30$. We used fewer solves at this high value of S in part to reduce the computational expense of the run, and in part because of how a third BVP generally did not modify the solution hugely (as in Fig. 1c).

Appendix B: Table of Runs

In Table I we list key properties of all simulations conducted in this work. The supercriticality, Rayleigh number, and resolution are reported. We report the simulation run time of the SE solutions and AE solutions, as well as the amount of time over which average measurements were taken, in freefall time units. The volume-averaged Nusselt number of the AE and SE solutions are shown. In the upper part of the table, information pertaining to 2D runs is reported, and below the double horizontal bars we report properties of all 3D runs.

[1] B. P. Brown, M. K. Browning, A. S. Brun, M. S. Miesch, and J. Toomre, "Persistent Magnetic Wreaths in a Rapidly Rotating Sun," Astrophys. J. **711**, 424–438 (2010), arXiv:1011.2831 [astro-ph.SR].

[2] N. A. Featherstone and B. W. Hindman, "The Spectral Amplitude of Stellar Convection and Its Scaling in the High-Rayleigh-number Regime," Astrophys. J. **818**, 32 (2016), arXiv:1511.02396 [astro-ph.SR].

[3] M. Viallet, I. Baraffe, and R. Walder, "Towards a new generation of multi-dimensional stellar evolution models: development of an implicit hydrodynamic code," Astronomy & Astrophysics **531**, A86 (2011), arXiv:1103.1524 [astro-ph.IM].

[4] M. Viallet, I. Baraffe, and R. Walder, "Comparison of different nonlinear solvers for 2D time-implicit stellar hydrodynamics," Astronomy & Astrophysics **555**, A81 (2013), arXiv:1305.6581 [astro-ph.SR].

[5] M. Viallet, T. Goffrey, I. Baraffe, D. Folini, C. Geroux, M. V. Popov, J. Pratt, and R. Walder, "A Jacobian-free Newton-Krylov method for time-implicit multidimensional hydrodynamics. Physics-based preconditioning for sound waves and thermal diffusion," Astronomy & Astrophysics **586**, A153 (2016), arXiv:1512.03662 [astro-ph.IM].

[6] D. Lecoanet, B. P. Brown, E. G. Zweibel, K. J. Burns, J. S. Oishi, and G. M. Vasil, "Conduction in Low Mach Number Flows. I. Linear and Weakly Nonlinear Regimes," Astrophys. J. **797**, 94 (2014), arXiv:1410.5424 [astro-ph.SR].

[7] E. H. Anders and B. P. Brown, "Convective heat transport in stratified atmospheres at low and high Mach number," Physical Review Fluids **2**, 083501 (2017), arXiv:1611.06580 [physics.flu-dyn].

[8] B. Bordwell, B. P. Brown, and J. S. Oishi, "Convective Dynamics and Disequilibrium Chemistry in the Atmospheres of Giant Planets and Brown Dwarfs," Astrophys. J. **854**, 8 (2018), arXiv:1802.03026 [astro-ph.EP].

[9] M. Stix, "On the time scale of energy transport in the sun," Solar Physics **212**, 3–6 (2003).

TABLE I. Simulation parameters

S	Ra	nz	nx, ny	$t_{\rm therm}$	$t_{\rm avg}$	$\mathrm{Nu_{SE}}$	$\mathrm{Nu_{AE}}$
$10^{1/3}$	$2.79 \cdot 10^3$	32	64	52.8	100	1.46	1.46
$10^{2/3}$	$6.01 \cdot 10^3$	32	64	77.6	100	1.95	1.95
10^{1}	$1.30 \cdot 10^4$	32	64	114	100	2.43	2.42
$10^{1+1/3}$	$2.79 \cdot 10^4$	32	64	167	100	2.54	2.54
$10^{1+2/3}$	$6.01 \cdot 10^4$	32	64	245	100	3.14	3.14
10^{2}	$1.30 \cdot 10^5$	64	128	360	100	3.8	3.8
$10^{2+1/3}$	$2.79 \cdot 10^5$	64	128	528	100	4.71	4.71
$10^{2+2/3}$	$6.01 \cdot 10^5$	64	128	776	100	5.5	5.5
10^{3}	$1.30 \cdot 10^6$	128	256	$1.14 \cdot 10^3$	200	6.4	6.33
$10^{3+1/3}$	$2.79 \cdot 10^6$	128	256	$1.67 \cdot 10^3$	500	6.87	6.95
$10^{3+2/3}$	$6.01 \cdot 10^6$	256	512	$2.45 \cdot 10^3$	500	7.54	7.59
10^{4}	$1.30 \cdot 10^7$	256	512	$3.60 \cdot 10^3$	500	8.83	8.83
$10^{4+1/3}$	$2.79 \cdot 10^7$	256	512	$5.28 \cdot 10^3$	500	10.13	10.14
$10^{4+2/3}$	$6.01 \cdot 10^7$	256	512	$7.76 \cdot 10^3$	500	11.65	11.69
10^{5}	$1.30 \cdot 10^8$	512	1024	$1.14 \cdot 10^4$	500	14.02	14.18
$10^{5+1/3}$	$2.79 \cdot 10^8$	512	1024	$1.67 \cdot 10^4$	500	–	16.21
$10^{5+2/3}$	$6.01 \cdot 10^8$	512	1024	$2.45 \cdot 10^4$	500	–	18.58
10^{6}	$1.30 \cdot 10^9$	1024	2048	$3.60 \cdot 10^4$	500	–	22.13
10^{7}	$1.30 \cdot 10^{10}$	2048	4096	$1.14 \cdot 10^5$	200	–	40.78
10^{1}	$1.30 \cdot 10^4$	32	64×64	114	100	2.42	2.42
10^{2}	$1.30 \cdot 10^5$	64	128×128	360	100	3.97	4
10^{3}	$1.30 \cdot 10^6$	128	256×256	$1.14 \cdot 10^3$	500	6.27	6.27
10^{4}	$1.30 \cdot 10^7$	256	512×512	$3.60 \cdot 10^3$	500	9.92	9.88

[10] H. Johnston and C. R. Doering, "Comparison of Turbulent Thermal Convection between Conditions of Constant Temperature and Constant Flux," Phys. Rev. Lett. **102**, 064501 (2009), arXiv:0811.0401 [physics.flu-dyn].

[11] R. Verzicco and R. Camussi, "Transitional regimes of low-Prandtl thermal convection in a cylindrical cell," Physics of Fluids **9**, 1287–1295 (1997).

[12] N. E. Hurlburt, J. Toomre, and J. M. Massaguer, "Two-dimensional compressible convection extending over multiple scale heights," Astrophys. J. **282**, 557–573 (1984).

[13] L.-A. Couston, D. Lecoanet, B. Favier, and M. Le Bars, "Dynamics of mixed convective-stably-stratified fluids," Physical Review Fluids **2**, 094804 (2017), arXiv:1709.06454 [physics.flu-dyn].

[14] A. Brandenburg, K. L. Chan, Å. Nordlund, and R. F. Stein, "Effect of the radiative background flux in convection," Astronomische Nachrichten **326**, 681–692 (2005), astro-ph/0508404.

[15] R. J. A. M. Stevens, D. Lohse, and R. Verzicco, "Prandtl and Rayleigh number dependence of heat transport in high Rayleigh number thermal convection," Journal of Fluid Mechanics **688**, 31–43 (2011), arXiv:1102.2307 [physics.flu-dyn].

[16] N. E. Hurlburt, J. Toomre, and J. M. Massaguer, "Nonlinear compressible convection penetrating into stable layers and producing internal gravity waves," Astrophys. J. **311**, 563–577 (1986).

[17] E. A. Spiegel and G. Veronis, "On the Boussinesq Approximation for a Compressible Fluid." Astrophys. J. **131**, 442 (1960).

[18] F. Cattaneo, N. H. Brummell, J. Toomre, A. Malagoli, and N. E. Hurlburt, "Turbulent compressible convection," Astrophys. J. **370**, 282–294 (1991).

[19] L. Korre, N. Brummell, and P. Garaud, "Weakly non-Boussinesq convection in a gaseous spherical shell," Phys. Rev. E **96**, 033104 (2017), arXiv:1704.00817 [physics.flu-dyn].

[20] K. Burns, G. Vasil, J. Oishi, D. Lecoanet, and B. Brown, "Dedalus: Flexible framework for spectrally solving differential equations," Astrophysics Source Code Library (2016), ascl:1603.015.

[21] U. M. Ascher, S. J. Ruuth, and R. J. Spiteri, "Implicit-explicit Runge-Kutta methods for time-dependent partial differential equations," Applied Numerical Mathematics **25**, 151–167 (1997).

[22] David Goluskin, Hans Johnston, Glenn R. Flierl, and Edward A. Spiegel, "Convectively driven shear and decreased heatflux," J. Fluid Mech. **759**, 360–385 (2014).

[23] J. Otero, R. W. Wittenberg, R. A. Worthing, and C. R. Doering, "Bounds on Rayleigh Bénard convection with an imposed heat flux," J. Fluid Mech. **473**, 191–199 (2002).

[24] J. V. Wall and C. R. Jenkins, *Practical Statistics for Astronomers, by J. V. Wall , C. R. Jenkins, Cambridge, UK: Cambridge University Press, 2012* (2012).

[25] David Goluskin, *Internally Heated Convection and Rayleigh-Bénard Convection* (Springer International Publishing, 2016).

[26] A. Brandenburg, "Stellar Mixing Length theory with entropy rain," arXiv (2016), arXiv:1504.03189.
[27] B. Paxton, L. Bildsten, A. Dotter, F. Herwig, P. Lesaffre, and F. Timmes, "Modules for Experiments in Stellar Astrophysics (MESA)," The Astrophysical Journal Supplement Series **192**, 3 (2011), arXiv:1009.1622 [astro-ph.SR].
[28] W. D. Arnett, C. Meakin, M. Viallet, S. W. Campbell, J. C. Lattanzio, and M. Mocák, "Beyond Mixing-length Theory: A Step Toward 321D," Astrophys. J. **809**, 30 (2015), arXiv:1503.00342 [astro-ph.SR].
[29] A. Cristini, C. Meakin, R. Hirschi, D. Arnett, C. Georgy, and M. Viallet, "Linking 1D evolutionary to 3D hydrodynamical simulations of massive stars," Physica Scripta **91**, 034006 (2016), arXiv:1601.01572 [astro-ph.SR].